

Research Article

Determination of the Baseline in the IR Spectra of External Reflection of Polymers for 3D Objects

V. M. Zolotarev^{1*}, N. N. Rozanov²

¹Department of Physical Optics and Spectroscopy, ITMO University, St. Petersburg, Russia

²A.F. Ioffe Institute, St. Petersburg, Russia

E-mail: vm-zolotarev@mail.ru

Received: 11 February 2025; **Revised:** 16 April 2025; **Accepted:** 18 April 2025

Abstract: A methodology for forming a baseline of infrared (IR) spectra of external reflection for objects with a smooth non-flat surface is proposed. The procedure for forming a baseline provides conditions for the correct application of the Kramers-Kronig method. The method is tested in determining the complex refractive index of 3D objects made of polymeric materials.

Keywords: baseline, reflectance spectra, polymers, 3D objects

1. Introduction

Polymer products are widely used in various fields of science and technology: optics and photonics, mechanical engineering and aircraft manufacturing, as well as in medicine and biology [1]. IR transmission spectroscopy methods are traditionally used to develop and study new polymeric materials. However, with the advent of modern Fourier spectrophotometers with a high signal-to-noise ratio (S/N), external specular reflection IR-spectroscopy methods have become increasingly used to identify different types of polymers [2–5]. The use of external reflection (R) methods to identify different polymers significantly simplifies the sample preparation procedure. However, quantitative research methods using external reflectance spectroscopy R , especially when applied to real industrial products, encounter difficulties. This is because the configuration of industrial polymer 3D objects often differs from a flat surface. The shape relief of the reflecting surface affects the course of the spectral dependence of R . Since all models of mathematical processing of the results of reflection measurements use a flat surface boundary, deviation from these conditions imposes restrictions on the application of the Kramers-Kronig method for processing the real spectrum of R . To eliminate the influence of the object shape on the spectrum of R , it is proposed to introduce a correction using a standard software platform for data collection and data management, which controls Fourier IR spectrometers [6–8]. The typical menu (*Processing*) includes the *Baseline Correction* option, using the “rubberband line” option, for example, Spectrum 10 (Perkin Elmer, USA), OPUS 7.0 (Bruker Optiks, Germany), OMNIC Spectra-2.1 (Thermo FS, USA). However, the typical “rubberband line” procedure is designed to correct the background of the spectra: absorption A (or transmission T) [9–11], attenuated total reflection (ATR) spectra, and diffuse reflectance infrared Fourier transform (DRIFT) and is not directly intended for the correction of external reflectance spectra (R).

Copyright ©2025 V. M. Zolotarev, et al.

DOI:

This is an open-access article distributed under a CC BY license
(Creative Commons Attribution 4.0 International License)

<https://creativecommons.org/licenses/by/4.0/>

The use of typical algorithms [6–8] for the correction of the baseline in external reflectance spectra during their subsequent processing by the Kramers-Kronig method leads to a distortion of the dispersion behavior n at the edges of the spectral range of wavelengths λ and affects the ratio of the intensities of the absorption bands. It should be noted that the use of the typical “rubberband line” correction procedure, which is applied to the A spectrum, when applied to the processing of the R spectrum, the position of the maxima of the main absorption bands changes practically little. This allows using this method of correcting the R spectrum for qualitative analysis tasks, for example, polymer identification [6–8].

If the sample surface is smooth but does not meet certain requirements for surface flatness, phase-sensitive methods of external reflection R [12, 13] or classical dispersion analysis [14] are used in small areas of the spectrum. These methods allow one to calculate the complex refractive index ($\hat{n} = n - i \cdot k$), where n and k are defined as the refractive and absorption indices, respectively. In this case, the absorption coefficient ($K\text{cm}^{-1}$) is determined from the ratio: $T = \lg(Kd)$, where T is the transmission, d is the film thickness and $K = 4\pi k/\lambda$. The wavelength λ is related to the wavenumber ν by the relation $\nu = 1/\lambda$. In the case of polymers, distortions introduced into the R spectrum due to deviation of the sample shape from the ideal plane often prevent reliable data from being obtained for the absorption index k values. Often, these deviations in the absorption spectra calculated by different methods for real polymer samples are especially clearly manifested in the short-wavelength region λ for large values of $k \geq 0.1$ [13–16].

This work aims to substantiate a method for correcting the experimental IR reflection spectrum in the region of the normal to the surface of a 3D sample, which allows, use a “baseline”, to correct the influence of the sample shape on its specular reflection spectrum.

2. Samples and equipment

Samples made of standard polymeric material were selected for the study: polystyrene (PS) and polymethyl methacrylate (PMMA). These materials are often used for modeling the optical properties of various objects [17–19]. Industrial samples of polymer products in the form of cylindrical tubes of different diameters were used. The thickness of the tube is indicated in Table 1. Along with samples with a cylindrical surface, complex-shaped polyethylene (high density polyethylene (HDPE), low density polyethylene (LDPE)) products were studied, see Table 1.

Table 1. Parameters of samples and surface roughness dimensions Ra

Samples	Surface shape	Surface dimensions (mm)	Tube thickness (mm)	Surface roughness parameter Ra (nm) [20]	Surface condition
PS	Cylindrical	External diameter of the tube = 60	6	-	Long-term storage in air
	Plate	60 × 60	7	1.3	Fresh surface
PMMA	Cylindrical	External diameter of the tube = 80	5	-	Fresh surface
	Plate	60 × 60	8	0.4	Fresh surface
LDPE	Plate (oval edges)	50 × 30	5	11.1	Contacted with chemicals
HDPE	Elongated (deformed) ellipsoid	halfaxes $\approx 120 \times 25 \times 20$	≈ 40	2.5	Long-term storage in air

The choice of PS and PMMA objects was due to the widespread use of these polymers for photonics problems, as well as for modeling the optical properties of various objects [18–21]. Data for the complex refractive index of PS and

PMMA polymers in the IR region were obtained mainly for films [21–26]. Therefore, it was necessary to use typical industrial supplies of massive polymer plates (5–8 mm), which were used as samples. For these thick plates, independent data for the complex refractive index were obtained for comparison with 3D tube samples, see Table 1.

For HDPE and LDPE polyethylene, the available data on the absorption value k are very limited and vary greatly in value [22–26], which is due to the different ratios of the amorphous and crystalline phases in the studied samples. For example, according to [26], the $-lgR$ value (proportional to the absorption index k) for various industrial polyethylene films obtained by the ATR method in the IR absorption band of $2,925\text{ cm}^{-1}$ can change by 3.5 times. The difference in the $-lgR$ value for polyethylene films of different compositions is determined by their density (kg/m^3), which depends on crystallinity. Reflectivity measurements of 3D samples were carried out using a Bruker TENSOR 27 IR Fourier spectrometer, spectral resolution 2 cm^{-1} , number of scans 50. The position of the 3D samples was controlled by the largest value of the reflected signal. When measuring the reflection from samples whose shape differs from a flat plate, the recommendations for working with non-standard samples on an IR Fourier spectrometer were taken into account [27].

2.1 Method for determining the “baseline” in the external reflection spectrum

The geometry of the scheme for reflecting an IR beam from a non-flat smooth cylindrical sample is shown in Figure 1. The aperture of the incident α beam, when reflecting from a cylindrical object, the beam divergence increases- A . As the diameter of the cylinder D decreases, the intensity of the reflected IR beam decreases.

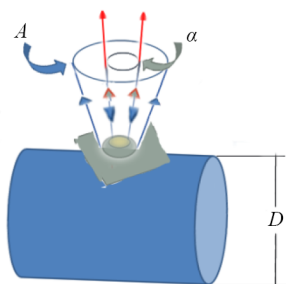


Figure 1. Geometry of the scheme of reflection of the beam of IR radiation from a smooth cylinder. α -aperture of the incident beam: downward direction of the inner blue arrows-incident beam, upward direction of the red-blue wide arrows-beam reflected from the conventional horizontal plane perpendicular to the radius of the cylinder $D/2$; A -aperture of the beam reflected from the surface of the cylinder (outer blue arrows), red arrows-useful part of the beam reflected from the surface of the cylinder entering the Fourier spectrometer, D -diameter of the cylindrical sample

The concept of “baseline” is used when correcting the normal reflection spectrum from smooth non-flat objects. To correct such a reflection spectrum, the baseline must be a smooth curve dependent on the wavelength λ . This smooth curve is located at a certain distance from the reflection spectrum, which depends on the integral intensity of the reflection bands of the object. With increasing λ , the distance between the reflection spectrum and the baseline will increase, depending on the intensity of the spectral bands, see Figure 2. The convex shape of the surface of 3D samples leads to a smooth increase in the reflection spectrum $R(\lambda)$ with increasing λ . It is assumed that the angle of incidence near the normal remains constant, i.e. does not depend on λ . The slope of the spectrum $R(\lambda)$ depends on the ratio D/λ . For a fixed size D , with increasing λ , the intensity of the spectrum $R(\lambda)$ smoothly increases, see Figure 2. For 3D samples, the reflection spectrum $R(\lambda)$ depends on the shape and radius of the local area of the reflecting surface.

To correct the $R(\lambda)$ spectrum of a polymer object with a complex surface, one can use a “baseline” whose construction differs from the baseline used in absorption spectroscopy [18–22]. The rationale for forming a “baseline” for the $R(\lambda)$ spectrum can be conveniently examined using classical dispersion analysis (CDA) for a typical polymer with a small number of bands in the reflection spectrum.

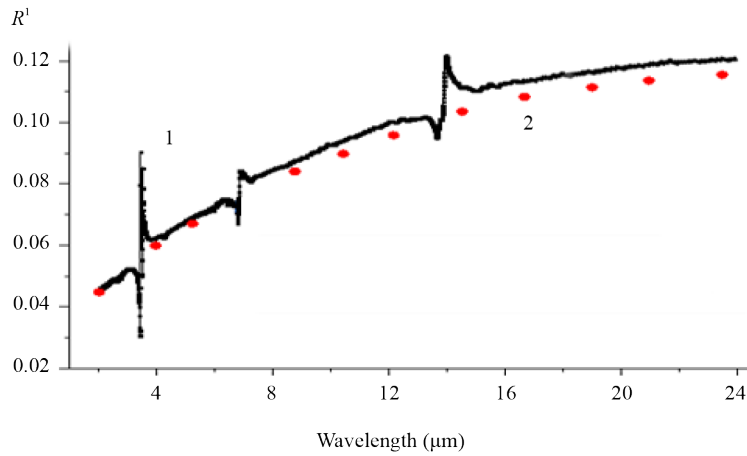


Figure 2. 1-experimental reflection spectrum $R^l(\lambda)$ of a plate with a non-flat surface (LDPE polyethylene), see Table 1. 2-intermediate points for constructing the “baseline”

2.2 Method of correction of experimental spectrum R

Classical dispersion analysis relations: equations (1) and (2) are presented by Lorentz-Lorenz and describe the value of the complex permittivity $\tilde{\epsilon} = \epsilon_r - i\epsilon_{Im}$, where $\epsilon_r(\nu) = n^2(\nu) - k^2(\nu)$, $\epsilon_{Im} = 2n(\nu)k(\nu)$ using a set of damped oscillators [9]:

$$n^2(\nu) - k^2(\nu) = \epsilon_\infty + \sum_j F_j \frac{\nu_j^2 - \nu^2}{(\nu_j^2 - \nu^2)^2 + \Gamma_j^2 \nu^2} \quad (1)$$

$$2n(\nu)k(\nu) = \sum_j \frac{F_j \Gamma_j \nu}{(\nu_j^2 - \nu^2)^2 + \Gamma_j^2 \nu^2} \quad (2)$$

The value $\epsilon_r = \epsilon_\infty = n_\infty^2$ (high-frequency component) determines the base level, j is an individual oscillator centered at frequency ν_j , the parameter F_j is related by the relation $F_j = f_j N e^2 / (\pi c^2 m)$ with the oscillator strength f_j , Γ_j is related to the oscillator damping γ , $\Gamma_j = \gamma_j / (2\pi c)$, where e denotes the electron charge, m is the mass electron, c is the speed of light in vacuum, N is the number of oscillators, $j = 1, 2, \dots, N$.

In the external reflection spectrum $R(\lambda)$ of the polymer, the “baseline” for a massive polymer 3D sample (see Figure 3) is similar to the “baseline” in the spectrum of the polymer dispersion curve $n(\lambda)$ [18–22]. As can be seen from Figure 3, in the spectral sections (regions) following the reflection bands R , the distance ΔR between the “baseline” and the curve R increases. The value of ΔR is proportional to the area of the band R , which for typical polymer bands $k(\lambda) \leq 0.3$ correlates with the course of dispersion $n(\lambda)$. Thus, as the frequency ν increases, the distance ΔR between the “baseline” and the spectrum R will increase. The “baseline” will have a fixed point in the high-frequency part of the spectrum R and will smoothly increase the value of ΔR moving away from the curve R as λ increases, see Figure 3.

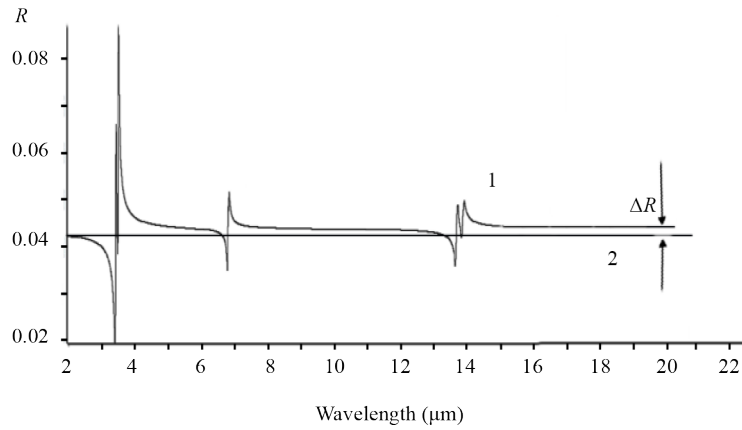


Figure 3. Model spectrum of the reflection coefficient R of polyethylene for a normal angle of incidence, the calculation was performed by the CDA method: the number of oscillators is 7, the parameters of the oscillators are [22], ΔR is the distance between the horizontal “baseline” and the spectrum R in the long-wave region

The features of the dependence of the experimental reflection spectrum of a 3D sample with a complex surface require correction of the obtained spectrum, which is necessary for subsequent matte processing. In practice, a relative method for measuring the reflection coefficient R from the surface of a flat sample is usually used. In this case, we have the relationship: $R = I_s/I_e \times R_{ET}$, where R is the reflection coefficient for a flat surface of a polymer sample, I_s is the signal from the sample, I_e is the signal from the comparison standard, R_{ET} is the reflection coefficient for the comparison standard. When measuring reflection for a 3D sample, the experimental spectrum R^1 differs from the spectrum of a flat sample $R \neq R^1$. To reduce the measured R^1 to the value of R for a flat sample, it is necessary to correct the measured spectrum R^1 using a correction that takes into account the effect of the curvature of the 3D sample surface. In this case, the reconstruction of the R spectrum for a 3D sample can be presented as:

$$R = R^1 \times \Pi(v, \phi), \quad (3)$$

where $\Pi(v, \phi) = a(\phi) \times M(v, \phi)$ is a correction factor, $a(\phi)$ is a constant coefficient depending on the local shape of the surface interacting with the incident IR radiation beam, $M(v, \phi)$ is a variable coefficient depending on the frequency and local shape of the 3D-sample surface. By correcting the experimental value of R^1 based on equation (3), we can obtain the R spectrum and subsequently use the Kramers-Kronig relations or classical dispersion analysis (CDA).

The two main reference points for forming the “baseline” required for constructing $\Pi(v, \phi)$ for the initial high-frequency point of the spectrum (R_∞) and the low-frequency point (R_0) for typical polymers can be obtained from reference data for R_∞ and n^2_0 [22–24, 28]. For polymers, the value of n_∞ can be represented in the first approximation by the values of n_D for the visible region [22], and the constant n^2_0 is replaced by the value of the permittivity ϵ_r [28] for a given polymer. It is assumed that the calculated values of R_∞ and R_0 correspond to the initial and final points of the calculated spectrum R , respectively. Since $k = 0$ for these frequency ranges, knowing n_∞ and n_0 , one can find the correct values for R_∞ and R_0 of the polymer [5] using Eq. (4):

$$R = \frac{(n-1)^2 + k^2}{(n+1)^2 + k^2} \quad (4)$$

The intermediate points between the fixed points with known values of R_∞ and R_0 , required for correcting the initial spectrum R^1 , are found manually empirically using the “baseline” formation, see Figure 2. Then, interpolation

is applied using a spline to find the spectrum of the correction factor $\Pi(\nu, \phi)$. After determining R , the subsequent stages of calculating the spectrum of the complex refractive index are conveniently carried out using the Kramers-Kronig method [9]:

$$\phi(\nu) = -\frac{2\nu}{\pi} \int_{\nu_H}^{\nu_k} \frac{\ln \sqrt{R}(\nu^*)}{\nu^{*2} - \nu^2} d\nu^*, \quad (5)$$

where $\phi(\nu)$ is the phase of the reflected radiation, ν_H and ν_k are the initial and final points of integration of the spectrum $R(\nu)$, ν is the current frequency for which the value of ϕ is calculated, ν^* is the frequency that serves as the integration variable.

$$\vec{r} = \frac{1 - n - ik}{1 + n + ik} = |r|e^{i\phi}, \quad |r| = \sqrt{R} \quad (6)$$

r -is the amplitude reflection coefficient.

By measuring $R(\nu)$ and calculating ϕ , $n(\nu)$ and $k(\nu)$ can be determined [4].

The results of calculating $n(\nu)$ and $k(\nu)$ of a 3D object based on the corrected spectrum R are compared with the databases of $n(\nu)$ and $k(\nu)$ spectra of polymers [22–24]. To achieve good agreement between the results of calculating the $n(\nu)$ and $k(\nu)$ values of a 3D object and the databases, it is necessary to manually refine the parameters $\Pi(\nu, \phi)$ of the “baseline” approximately 3-5 times.

Another method for calculating the spectrum of the complex refractive index is based on machine modeling using the CDA. With this method, the original spectrum $R^1(\nu)$ can be reconstructed in the first approximation into the spectrum $R(\nu)$ by constructing a “baseline” for standard tools [2–4]. The frequency values ν_j for the maxima of the absorption bands are found using the primary processing of $R^1(\nu)$ using the Kramers-Kronig method.

Then, using the CDA method, $n_{exp}(\nu)$ and $k_{exp}(\nu)$ of the 3D-object are calculated from the spectrum $R(\nu)$ and compared in machine mode with the known data $n_{model}(\nu)$ and $k_{model}(\nu)$, obtained mainly for polymer films [24, 25]. To calculate the data $n_{model}(\nu)$ and $k_{model}(\nu)$, the known number of oscillators N and the frequency values ν_j are entered into the CDA program in advance. For rapid convergence of the calculation results, it is advisable to specify the range of k_j values for the most intense bands in the spectrum R . In the process of machine search, the data $n_{exp}(\nu)$ and $k_{exp}(\nu)$, calculated using the CDA program from the reconstructed spectrum $R(\nu)$, are compared with the values of $n_{model}(\nu)$ and $k_{model}(\nu)$ from the reference data [22–24, 29]. This calculation method, when the search is carried out for a fixed number of bands ν_j , simplifies the finding of $n_{exp}(\nu)$ and $k_{exp}(\nu)$, but the information is lost for weak impurity IR bands that may be present in the surface layer [13, 22, 30, 31].

The magnitude of the difference between the model spectrum and the experimental one is characterized using the residual function Q . For example, for the case of analyzing the spectrum $k_{exp}(\nu)$, it is convenient to use the residual function Q of the form:

$$Q^2 = \frac{1}{\nu_H - \nu_K} \int_{\nu_H}^{\nu_K} [k_{model}(\nu) - k_{exp}(\nu)]^2 d\nu, \quad (7)$$

where ν_H , ν_K -the boundaries of the range occupied by the analyzed spectrum $k(\nu)$. The accuracy characteristics of the calculated parameter $k_{exp}(\nu)$ for PS and PMMA samples were compared with reliable literature values of $k_{model}(\nu)$ [21, 29]. With a 3-5-fold iteration of the value $M(\nu, \phi)$ and subsequent calculation of $k_{exp}(\nu)$, the value of the parameter Q^2 is $1 \times 10^{-4} - 1 \times 10^{-6}$. The value of Q^2 mainly depends on the surface condition of the 3D sample and the experience of the researcher. For fresh PS and PMMA samples in the form of plates, the parameter Q^2 for the calculated spectrum $k_{exp}(\nu)$ was 2×10^{-6} , while for LDPE and HDPE polyethylene samples, the value of Q^2 was significantly larger $\approx 2 \times 10^{-4}$. The

relatively large value of Q^2 for polyethylene is associated with the degradation of the surface layer of these two samples, see Table 1.

3. Discussion of results

3.1 Surface research of bulk 3D-objects PS, PMMA

Figure 4 shows the experimental $R(\nu)$ and corrected $R^1(\nu)$ spectra of 3D objects made of polymers (PS, PMMA) in the form of cylindrical tubes of different diameters with a smooth surface. The $R(\nu)$ spectra were obtained in the manual “baseline” formation mode with a 3-fold iteration of the correction parameter $M(\nu, \phi)$. The reference constant coefficient $a(\phi)$ was determined for PS and PMMA based on the known tabular values of n_∞ and n^2_0 [22, 28].

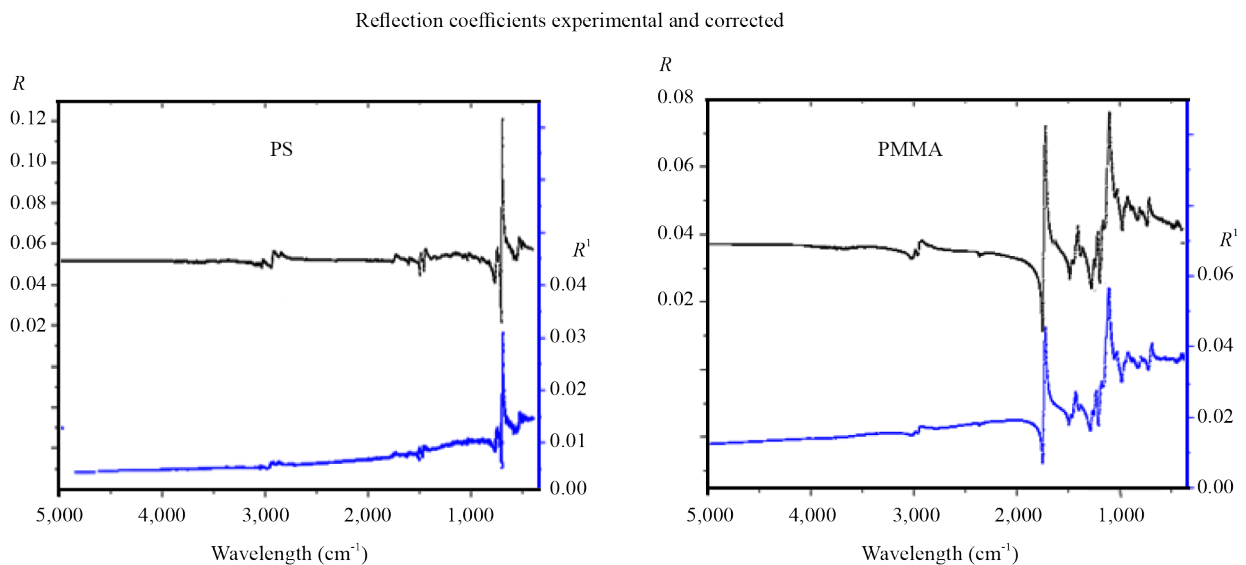


Figure 4. Reflection coefficients $R^1(\nu)$ and $R(\nu)$ for industrial cylindrical tubes made of PS and PMMA see Table 1

When calculating $n_{exp}(\nu)$ and $k_{exp}(\nu)$ for PS and PMMA samples, we proceeded from a simplified optical model: industrial cylindrical tubes have smooth surfaces and border on the air environment. The results of $n_{exp}(\nu)$ and $k_{exp}(\nu)$ calculations obtained by processing the $R(\nu)$ spectrum in the range of 5,000-400 cm^{-1} by the kk method are shown in Figure 5.

The obtained values of $n_{exp}(\nu)$ and $k_{exp}(\nu)$ for the 3D-sample PMMA are in good agreement with the result obtained for the model plate. On the other hand, the $k_{exp}(\nu)$ spectrum for the 3D-sample PS differs significantly from the spectrum for the model plates, see Figure 6. It should be noted that the values of $n(\nu)$ and $k(\nu)$ for polymers strongly depend on several conditions, such as the instrumental research method [31–35], sample preparation technology [31–34] and storage conditions [35–37], on which the surface condition depends. The differences are especially noticeable when comparing the $k(\nu)$ values of polymers for thin films [14, 16] and bulk samples [22, 31], see Tables 2, 3.

From the analysis of Tables 2 and 3, it is evident that the greatest differences in the k_{max} values of PS and PMMA polymers are observed for the strongest absorption bands. For less intense k bands in the PS spectrum, differences can also be seen between the 3D sample that was exposed to air for a long time (see Table 1) and the sample with a fresh surface [21], see Figure 6.

Refractive and absorption indices

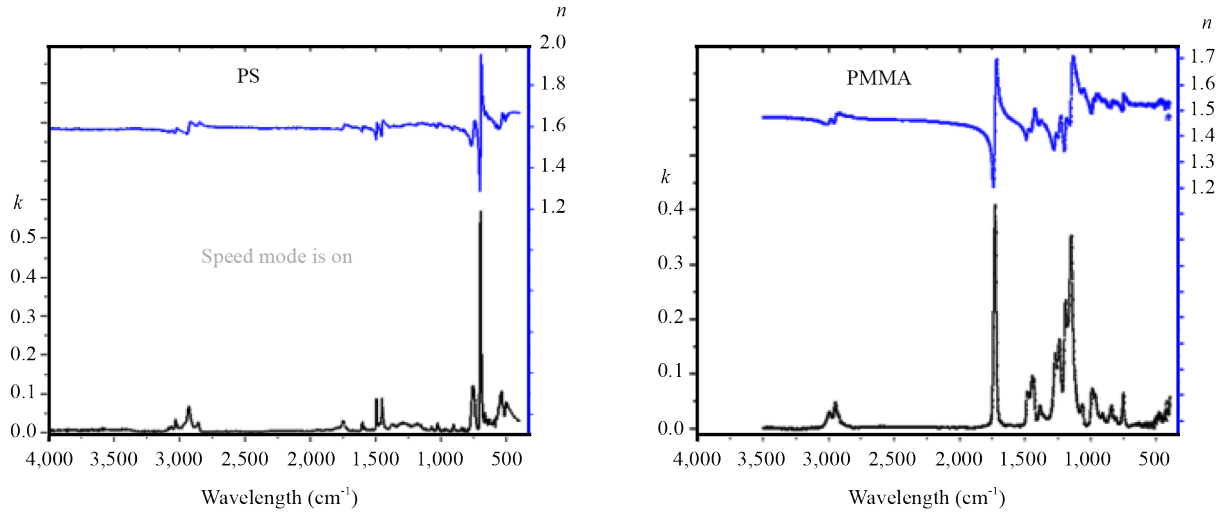


Figure 5. The refractive indices $n_{exp}(\nu)$ and absorption indices $k_{exp}(\nu)$ calculated by the kk method for industrial cylindrical tubes made of PS and PMMA are given in Table 1

Table 2. Absorption indices k_{max} for the main IR bands of PS

ν, cm^{-1}	[35]	[32]	[12]	[21]	[29]	This work
3,082	0.0101	0.02	0.012	0.011	0.0139	0.012
3,060	0.0144	0.03	0.017	0.0159	-	0.0146
3,026.5	0.0237	0.06	0.035	0.0331	0.0224	0.032
3,001.5	0.0063	-	-	0.0073	-	-
2,923	0.0294	0.0265	0.040	0.047	0.033	0.066
2,849.5	0.0108	0.009	0.013	0.017	0.013	0.025
1,943	0.0036	0.003	0.003	0.0041	0.0065	0.0075
1,801.5	0.0038	0.0026	0.0024	0.0034	0.0060	0.0104
1,601.5	0.0220*	0.0209	0.027	0.0278	0.0188	0.025
1,493	0.0407	0.067	0.075	0.0841	0.0381	0.088
1,451.5	0.0455	0.065	0.072	0.084	0.0499	0.090
1,371.5	0.0107	0.0078	0.010	0.017	0.0172	0.022
1,181.5	0.0099	0.0074	0.008	0.0086	-	0.025
1,154.5	0.0092	0.0071	0.006	0.0099	-	0.021
1,069.5	0.0139	0.0102	0.015	0.0129	0.0316	0.015
1,028	0.0243	0.0215	0.029	0.0281	0.0354	0.025
906.5	0.0168	0.0149	0.020	0.0162	0.0198	0.020
842	0.0076	0.0072	-	0.0064	0.0122	0.012
756.5	0.0951	0.0897	-	0.107	0.1048	0.12
700	0.1169	0.25*	-	0.543	0.3233	0.60
540.5	0.0663	0.0563	-	0.052	0.064	0.105

Note: k_{max} values (25, 35, 48, 51) were obtained for PS films, data for bulk PS [29] and the last column

Absorption indices of 3D-samples and flat plates

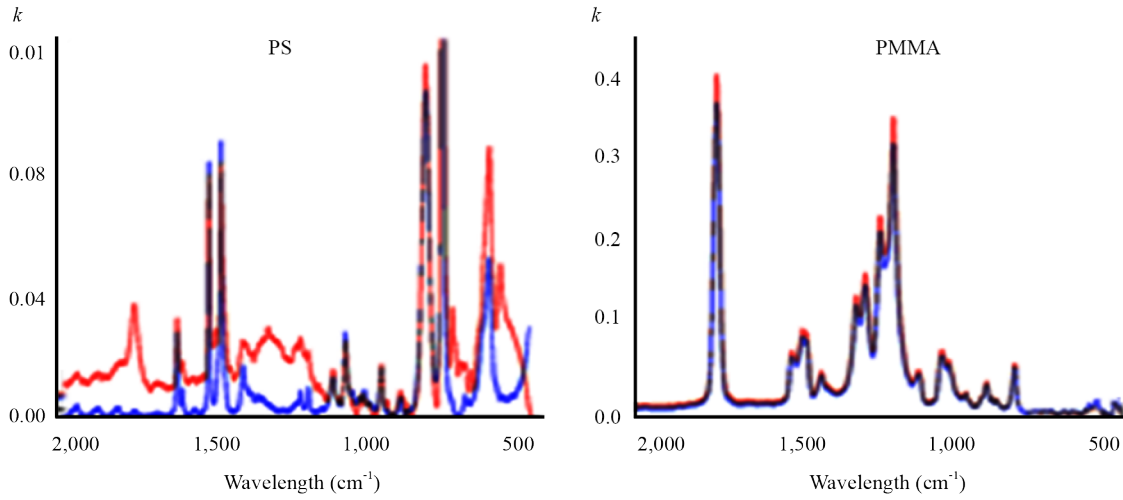


Figure 6. Absorption indices $k_{exp}(\nu)$ calculated by the kk method. PS: red line-cylindrical tube, blue line-comparison plate, see Table 1. PMMA: red line-cylindrical tube, blue line-comparison plate [29]

Table 3. Absorption indices k_{max} of the main IR bands of PMMA (bulk)

ν, cm^{-1}	[35]	[15]	[33]	[2]	[29]	This work
2,995	-	-	≈ 0.04	0.033	0.025	0.029
2,951	-	-	≈ 0.06	0.053	0.034	0.044
1,730	0.44	0.45	0.407	0.402	0.361	0.403
1,448	≈ 0.10	0.11	0.10	0.097	0.092	0.096
1,387	≈ 0.03	0.06	≈ 0.06	0.0403	0.038	0.044
1,270	0.08	0.26	0.14	0.149	0.116	0.136
1,241	0.14	0.18	0.18	0.168	0.149	0.165
1,192	0.19	0.265	0.24	0.237	0.216	0.236
1,150	0.33	0.41	0.329	0.357	0.329	0.348
989	0.058	0.076	0.085	0.067	0.0629	0.079
841	≈ 0.05	0.0419	0.05	0.036	0.0351	0.04
750	-	0.019	0.055	0.059	0.0448	0.06
483	-	-	≈ 0.03	≈ 0.014		≈ 0.033

The appearance of additional IR bands in the spectrum of the 3D-sample of the PS polymer in the region of vibrations of OH groups ($3,580, 3,400, 1,640 \text{ cm}^{-1}$) and various carbonyl groups (carbonyl band $1,740 \text{ cm}^{-1}$ C=O group, triplet $1,368, 1,287, 1,187 \text{ cm}^{-1}$ C-O-C group) indicates degradation of the surface layer of the sample under study. Changes in the chemical structure of the PS surface are associated with the effects of moisture, atmospheric oxygen, and ultraviolet rays [36]. In the spectrum of PMMA, the differences between the compared 3D image and the model plate were practically insignificant. Therefore, it was decided to compare the spectrum of the 3D-sample PMMA with the spectrum of the model plate from the work [29]. The observed differences in Figure 6 for the k_{max} values of PMMA between the compared spectra are associated with different spectral interval widths: in our work, we have 2 cm^{-1} , while in work [29] the interval width is 16 cm^{-1} . As a result of differences in spectral resolution, the intensity of the bands is reduced, and their half-width $\Delta\nu$

in the work [29] is noticeably larger, see Figure 6. For example, according to data [29], the IR bands of PMMA have a half-width of $1,493\text{ cm}^{-1}$ ($\Delta\nu = 19\text{ cm}^{-1}$), 756 cm^{-1} ($\Delta\nu = 32\text{ cm}^{-1}$), 700 cm^{-1} ($\Delta\nu = 20\text{ cm}^{-1}$), while according to our data (see Table 3), the corresponding bands have a width of $\Delta\nu = 6\text{ cm}^{-1}$, $\Delta\nu = 29\text{ cm}^{-1}$, $\Delta\nu = 9.5\text{ cm}^{-1}$, respectively.

3.2 Surface research of bulk 3D-objects LDPE and HDPE

The results of the studies of bulk 3D samples of different grades of LDPE and HDPE polyethylene showed a high degree of HDPE crystallinity and noticeable differences in the surface structure of the samples, see Figure 7 and Table 4.

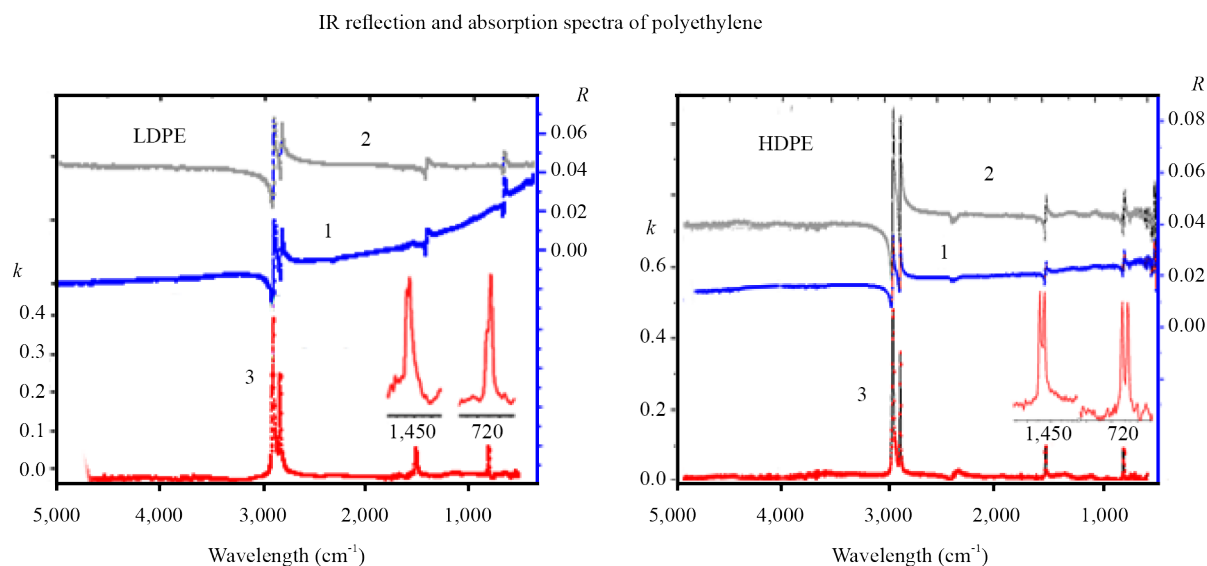


Figure 7. Spectra for polyethylene 3D-samples (LDPE and HDPE) with a non-planar outer smooth surface, see Table 1. 1-initial experimental spectrum R^1 ; 2-reflection spectrum R ; 3-absorption indices. The scale of the insert for the $1,450$ and 720 cm^{-1} bands is increased in the figure margins for clarity

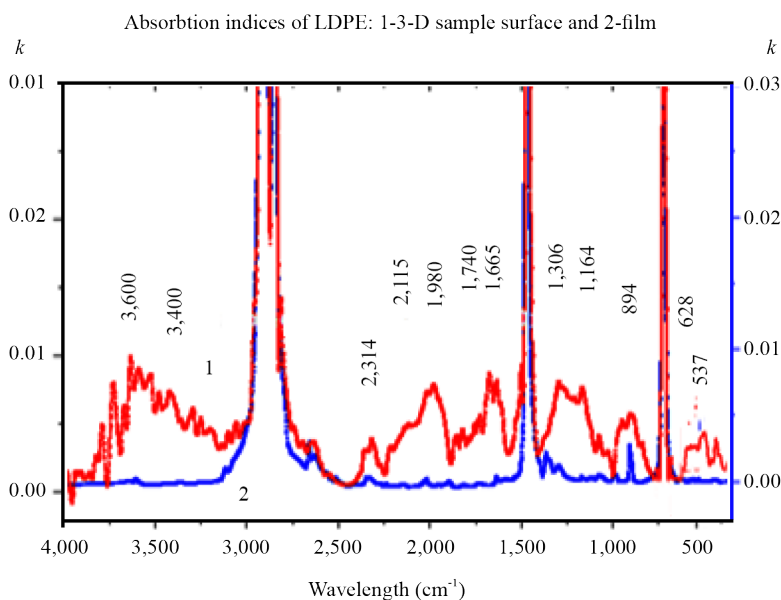


Figure 8. Absorption indices k of spectra: 1-LDPE polyethylene plate (see Figure 2 and Table 1), (red curve) spectrum obtained by processing spectrum R by the kk method. 2-LDPE film, (blue curve) spectrum of the film obtained by the transmission (T) method [24]

The reliability of measurements of small absorption values of LDPE with the correct use of a smooth baseline is demonstrated by the results of a comparison of the $k_{exp}(\nu)$ spectra in the background region for a 3D-object and a thin film, see Figure 8. Interpretation of the bands in the background region in the spectrum of a 3D-object is given in Table 4.

Table 4. IR absorption indices k_{max} of polyethylene LDPE and HDPE

Polyethylene Reference [38], cm^{-1}	LDPE	HDPE	Functional group	Copolymer PE-PEO [38, 39]
-	3,320	3,340	O-H asymmetric stretch	-
2,959	2,959	2,952	C-H asymmetric stretch in CH_3	PE, PEO
2,914	2,918	2,918	C-H asymmetric stretch in CH_2	PE
2,846	2,851	2,849	C-H symmetric stretch in CH_2	PE, PEO
-	2,314, 2,115, 1,980	2,015, 1,880	-C=C-symmetric stretch	PEO
-	1,665	1,615	OH_2 bend	-
-	1,600-1690	-	-C=O stretch	PEO
1,474	1,463	1,473, 1,463	CH_2 bend	PE
-	1,306	1,308	CH_3 bend	PEO
-	1,164, 1,080	1,040	C-O-C stretch	PEO
-	894	850	γ_r (CH_3)	PE
-	894	808	γ_r (CH_2)	PEO
720	720	720, 730	CH_2 rock	PE, PEO
-	628, 537, 450	640, 522	C-C-O bend	PEO

From the analysis of Figure 8 and Table 4, it is evident that the operating and storage conditions of the object have a noticeable effect on the degradation of the surface [36–39] of the non-flat LDPE polymer plate. The most characteristic vibration bands in the spectrum of Figure 8 are those that can be attributed to the C-O-C bonds $1,080, 900 \text{ cm}^{-1}$, C-C-O $628, 537, 450 \text{ cm}^{-1}$, and CH_2 $1,360, 1,342 \text{ cm}^{-1}$. The position of these bands in the k spectrum of the LDPE plate resembles the spectrum of the polyethylene-polyethylene-oxide copolymer [38, 39]. The presence of frequencies of $3,400$ and $1,640 \text{ cm}^{-1}$ indicates the hydrophilicity of the surface of the LDPE and HDPE samples. The frequencies and intensities of the polyethylene-oxide bands in the surface layer of LDPE and HDPE are slightly different (see Table 4), but in both cases, their intensity is significantly higher than that of similar bands in the spectrum of the film thickness obtained by the transmission method [24].

4. Prospects and limitations

The use of the “baseline” allows the future to test industrial polymer products of different configurations and shapes, for example, those with spherical, cylindrical, and ellipsoid surfaces. Correction of the original reflection spectrum of polymer 3D objects using the “baseline” allows to obtain objective quantitative data not only in the area of the main absorption bands but also improves the conditions for studying small absorption values. For this purpose, the software package of IR Fourier spectrometers should in the future include means for correcting the experimental reflection spectrum for 3D objects.

It is necessary to note the limitations associated with the use of the “baseline” that concern the study of samples with a rough surface. In this case, it is not recommended to process such a spectrum using the QC method. In addition, difficulties may arise when studying samples with complex surface relief, in which local relief deviations will be comparable with dimensions of approximately $\approx \text{mm}$. This is primarily due to diffraction-interference phenomena, and secondly, to the

low reflection of samples with such a surface profile. Another significant limitation concerns the correct choice of the optical model of the object under study. The presence of thin layers on the surface of objects requires appropriate means of matte processing, taking into account the presence of additional layers [5, 22]. For example, the presence of a thin surface layer in LDPE and HDPE samples requires clarification of the optical model of the reflective surface, especially when it is necessary to measure small values of $k \leq 0.01$. At the same time, it can be noted that the thin surface layer within the framework of the used simplified optical model in the region of weak absorption of the layer does not significantly affect the results obtained by the Kramers-Kronig method for the main bands of the polymer array, for which $k \geq 0.01$. The thin surface layer will have the most significant effect on the results of calculating the background intensity values of the bands, for which $k \leq 0.01$. At the same time, it is important to note that the position of the bands and their relative intensity related to the thin surface layer will have little effect on the choice of the optical model for a small limited spectral interval. The most radical way in a quantitative study of thin layers is to use a more correct optical model that takes into account the thin layer.

5. Conclusion

The described method for correcting the experimental spectrum of external reflection from 3D objects at a normal angle of incidence by constructing a “baseline” allows us to obtain quantitative values of the complex refractive index. Correction of the original reflection spectrum of objects with a complex configuration using a “baseline” improves the conditions for studying small absorption values. In particular, this allows us to study thin surface layers that arise during degradation processes during the aging of polymers. As an example of the usefulness of using a “baseline”, studies were carried out on the $n(\nu)$ and $k(\nu)$ values for different shapes of polymer 3D objects (PS, PMMA, LDPE, and HDPE). The obtained $k(\nu)$ values were compared with measurements performed for flat polished samples. It was shown that the surface layer of LDPE and HDPE polyethylene lying in the air contains functional groups characteristic of the polyethylene-polyethylene-oxide copolymer. Finally, it should be noted in agreement with the authors [5] that “the results of external reflectance measurements are highly dependent on the measurement conditions. The spectra obtained with this technique differ from those obtained with transmission spectroscopy. To obtain analytically useful information from external reflectance spectra, it is necessary to understand the physical phenomena responsible for the generation of the spectra and to carefully select the measurement conditions for a given sample”.

Acknowledgement

We express our gratitude to prof. B. Z. Volchek, Head of the Spectral Measurements Group at the Institute of Macromolecular Compounds of the Russian Academy of Sciences, for providing samples of polymer products and discussions on measuring IR Fourier reflectance spectra of 3D-samples of industrial polymer materials.

Conflict of interest

The authors declare no competing financial interest.

References

- [1] Cheremisinoff P. *Handbook of Engineering Polymeric Materials*. CRC Press; 1997.
- [2] Nishikida K, Nishio E, Hannah RW. *Selected Applications of Modern FT-IR Techniques*. Luxemburg: Gordon & Breach Sci. Publ.; 1995.
- [3] Stuart B, George WO. *Modern Infrared Spectroscopy*. UK: Wiley; 1996.

- [4] Fringeli UP. ATR and reflectance IR spectroscopy, applications. In: *Encyclopedia of Spectroscopy and Spectrometry*. Academic Press; 2017.
- [5] Handke M, Milosevic M, Harrick NJ. External reflection Fourier transform infrared spectroscopy: Theory and experimental problems. *Vibrational Spectroscopy*. 1991; 1(3): 251-262.
- [6] Bell J, Nel P, Stuart B. Non-invasive identification of polymers in cultural heritage collections: evaluation, optimisation and application of portable FTIR (ATR and external reflectance) spectroscopy to three-dimensional polymer-based objects. *Heritage Science*. 2019; 7: 95.
- [7] Picollo M, Bartolozzi G, Cucci C, Galeotti M, Marchiafava V, Pizzo B. Comparative study of fourier transform infrared spectroscopy in transmission, attenuated total reflection, and total reflection modes for the analysis of plastics in the cultural heritage field. *Applied Spectroscopy*. 2014; 68(4): 389-396.
- [8] Saviello D, Toniolo L, Goidanich S, Casadio F. Non-invasive identification of plastic materials in museum collections with portable FTIR reflectance spectroscopy: Reference database and practical applications. *Microchemical Journal*. 2016; 124: 868-877.
- [9] Leland KH, Mevik BH. *Baseline: Baseline Correction of Spectra*. 2023. Available from: <https://github.com/khliland/baseline/> [Accessed 15th January 2025].
- [10] Liland KH, Almoy T, Mevik BH. Optimal choice of baseline correction for multivariate calibration of spectra. *Applied Spectroscopy*. 2010; 64(9): 1007-1016.
- [11] Shen X, Ye S, Xu L, Hu R, Liu J, Liu W. Study on baseline correction methods for the Fourier transform infrared spectra with different signal-to-noise ratios. *Applied Optics*. 1998; 37(30): 7091-7095.
- [12] Graf RT, Koenig JL, Isida H. Optical constant determination of thin polymer films in the infrared. *Applied Spectroscopy*. 1985; 39(3): 405-408.
- [13] Korte E-H, Roseler A. Infrared ellipsometric determination of the optical constants of polytetrafluoroethylene. *Journal of Molecular Structure*. 2003; 661-662: 579-585.
- [14] Afanaseva N, Brame EG, Lockshin BV, Yakovlev VA. Infra-red spectra and optical constants of polytetrafluoroethylene films. *Polymer*. 1988; 29(5): 503-509.
- [15] Fajardo ME, Neel CH, Lacina DG. Using mid-infrared external reflectance spectroscopy to distinguish between different commercially produced poly[methyl methacrylate] (PMMA) samples-A null result. *AIP Conference Proceedings*. 2018; 1979: 130003.
- [16] Krynin AG, Khokhlov JA. Optical performances thermostabilised polyethyleneterephthalate film used for the functional materials of a glass cover. *Aviation Materials and Technologies*. 2013; S2: 4-9.
- [17] National Institute of Standards and Technology. *Standard Reference Materials Program*. USA.
- [18] Blümel R, Bağcıoğlu M, Lukacs R, Kohler A. Infrared refractive index dispersion of polymethyl methacrylate spheres from Mie ripples in Fourier-transform infrared microscopy extinction spectra. *Journal of the Optical Society of America A*. 2016; 33(9): 1687-1696.
- [19] de Silva K, Akbar PN, Blumel R. Space-resolved chemical information from infrared extinction spectra. *Research Square*. 2022; 11: 1-9.
- [20] Kolská Z, Řezníčková A, Švorčík V. Surface characterization of polymer foils. *e-Polymers*. 2011; 083: 1-13.
- [21] Myers TL, Tonkyn RG, Danby TO, Taubman MS, Bernacki BE, Birnbaum JC, et al. Accurate measurement of the optical constants n and k for a series of 57 inorganic and organic liquids for optical modeling and detection. *Applied Spectroscopy*. 2017; 72(4): 535-550.
- [22] Zolotarev VM, Morozov VN, Smirnova EV. *Optical Constants of Natural and Technical Media, The Handbook*. Leningrad: Khimiya; 1984.
- [23] Polyanskiy MN. Refractiveindex.info database of optical constants. *Scientific Data*. 2024; 11: 94.
- [24] Ashok J, Varaprasad PLH, Birh JR. Polyethylene (C₂H₄)_n. In: *Handbook of Optical Constants of Solids*. San Diego: Academic Press; 1991. p.957.
- [25] Wang Y, Abe Y, Matsumura Y, Miyagi M, Uyama H. Refractive indices and extinction coefficients of polymers for the mid-infrared region. *Applied Optics*. 1998; 37(30): 7091-7095.
- [26] Bredács M, Barretta C, Castillon LF, Frank A, Oreski G, Pinter G, et al. Prediction of polyethylene density from FTIR and Raman spectroscopy using multivariate data analysis. *Polymer Testing*. 2021; 104: 107406.
- [27] Bircha JR, Clarke FJJ. Fifty categories of ordinate error in Fourier transform spectroscopy. *Spectroscopy Europe/World*. 1995; 7(4): 16-22.

- [28] Ahmad Z. Polymer dielectric materials. *Dielectric Material*. 2012. Available from: <https://doi.org/10.5772/50638>.
- [29] Zhang X, Qiu J, Zhao JM, Li X. Complex refractive indices measurements of polymers in infrared bands. *Journal of Quantitative Spectroscopy and Radiative Transfer*. 2020; 252(3): 107063.
- [30] Rozanov NN, Zolotarev VM. Study of gradient characteristics of submicron surface layers of a solid using the ATR method. *Optics and Spectroscopy*. 1980; 49(5): 925-932.
- [31] Deev IA, Buryndin VG, Eltsov OS, Stoyanov OV. Calculation of the content of crystalline, amorphous and intermediate regions of polyethylene and its derivatives using IR Fourier spectroscopy data. *Bulletin of Kazan Technological University*. 2012; 6: 152-157.
- [32] Jitian S. Determination of optical constants of polystyrene films from IR reflection-absorption spectra. *Analele Universității "Eftimie Murgu" Reșita*. 2011; 18(1); 41-48.
- [33] Zolotarev VM, Volchek BZ, Vlasova EN. Optical constants of industrial polymers in the IR region. *Optics and Spectroscopy*. 2006; 101(5): 763-770.
- [34] Shimadzu Corp. *Measurement Methods for Films and Plastics*. Available from: <http://www.shimadzu.com/an/ftir/support/ftirtalk/talk11/intro.html> [Accessed 16th January 2025].
- [35] Richard S. *Reflection Measurements in IR Spectroscopy*. PerkinElmer, Inc.; 2021.
- [36] Achhammer BG, Reiney M, Reinhart FW. Study of degradation of polystyrene, using infrared spectrophotometry. *Journal of Research of the National Bureau of Standards*. 1951; 47(2): 116-125.
- [37] Martínez-Romo A, González-Mota R, Soto-Bernal JJ, Rosales-Candelas I. Investigating the degradability of HDPE, LDPE, PE-BIO, and PE-OXO films under UV-B radiation. *Journal of Spectroscopy*. 2015; 1: 586514.
- [38] Bergeron C, Perrier E, Potier A, Delmas G. A study of the deformation, network, and aging of polyethylene oxide films by infrared spectroscopy and calorimetric measurements. *International Journal of Spectroscopy*. 2012; 1: 432046.
- [39] Brogly M, Bistac S, Bindel D. Advanced surface FTIR spectroscopy analysis of poly(ethylene) block poly(ethylene oxide) thin film adsorbed on gold-substrate. *Applied Surface Science*. 2022; 603: 154428.